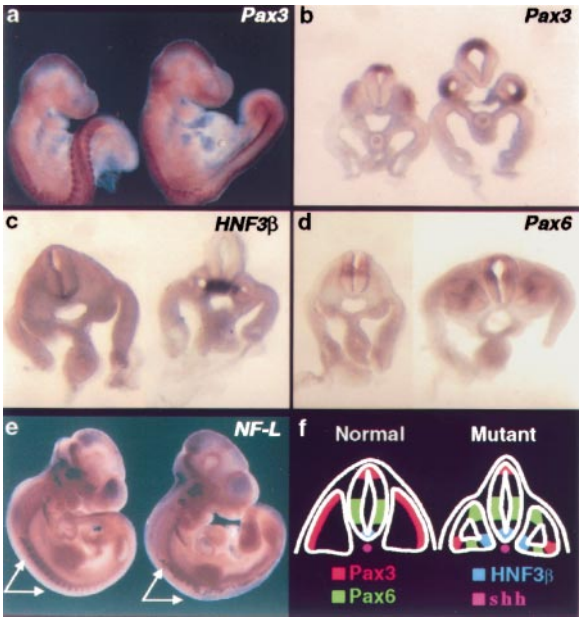

Figure 4 Expression of neural and neural/mesodermal markers in normal (left in each panel) and *Tbx6*-mutant (right in each panel) embryos at e9.5 (**a**–**c**) and e10.5 (**d**, **e**) as shown by whole-mount *in situ* hybridization (darker areas). **a**, *Pax3* is normally expressed in the dorsal neural tube and dermamyotome; in the mutant, a continuous line of expression is seen in the paraxial region and in the neural tube. **b**, A thick transverse section shows expression in the dorsal aspect of each paraxial tube. **c**, *HNF3β* and **d**, *Pax6* are normally expressed in the floor plate and lateral ventricular regions of the neural tube, respectively. In mutants, these neural markers indicate that the paraxial tubes are neural tubes radially arranged around the notochord. **e**, *Neurofilament-L* (*NF-L*) expression in the dorsal root ganglia (arrows) indicates disruption of the segmental pattern in mutants. **f**, Diagram of the expression patterns of neural-tube markers in normal and mutant embryos. shh, Sonic hedgehog.

Cells mutant for *fibroblast growth factor receptor-1*, when analysed in chimaeras, fail to ingress normally through the primitive streak and differentiate as ectopic neural-tube extensions of the endogenous neural tube[21,22]. Although fibroblast growth factors (FGFs) and some T-box proteins other than Tbx6 may function in the same signalling pathway[23], there is no evidence for direct interaction of FGF with Tbx6 in paraxial mesoderm. The fact that *Wnt3a* is expressed in *Tbx6*-mutant embryos indicates that *Wnt3a* is not directly regulated by *Tbx6*. We propose that all three of these genes are involved in interrelated signalling pathways involved in mesoderm specification during gastrulation, such that, in the absence of any one of the gene products, mutant cells destined to become mesoderm differentiate along a neural pathway. Furthermore, the fact that the paraxial neural tubes in *Tbx6* mutants arise from cells that have undergone ingression, mesenchyme formation and lateral migration indicates that mesodermal cell fate is regulated independently of the morphogenetic movements of gastrulation. □

Methods

Mouse *Tbx6* genomic clones were isolated from a genomic λ phage 129/Sv library (Stratagene). The targeting construct was generated by replacing a 1.9-kb *Spe*I/*Nco*I fragment with the neomycin-resistance gene under the control of the thymidine-kinase promoter (pMC1neo polyA, Stratagene). The targeting construct was linearized at a unique *Xba*I site before insertion into electroporated R1 ES cells[24]. We isolated DNA from cell clones and injected cells into blastocysts according to standard protocols[25]. Chimaeric mice were mated with C57BL/6J females, and offspring carrying the mutated allele, *Tbx6*^{tm1Pa}, were crossed to produce embryos for analysis. Expression of marker genes was studied using whole-mount *in situ* hybridization[26].

Received 8 August; accepted 13 November 1997.

1. Hogan, B., Holland, P. & Schofield, P. How is the mouse segmented. *Trends Genet.* **1,** 67–74 (1985).
2. Tam, P. P. L. & Trainor, P. A. Specification and segmentation of the paraxial mesoderm. *Anat. Embryol.* **189,** 2275–2305 (1994).
3. Chapman, D. L., Agulnik, I., Hancock, S., Silver, L. M. & Papaioannou, V. E. *Tbx6*, a mouse T-box gene implicated in paraxial mesoderm formation at gastrulation. *Dev. Biol.* **180,** 534–542 (1996).
4. Agulnik, S. I. *et al.* Evolution of mouse *T-box* genes by tandem duplication and cluster dispersion. *Genetics* **144,** 249–254 (1996).
5. Kispert, A. & Herrmann, B. G. The *Brachyury* gene encodes a novel DNA binding protein. *EMBO J.* **12,** 3211–3220 (1993).
6. Echelard, Y. *et al.* Sonic hedgehog, a member of a family of putative signaling molecules, is implicated in the regulation of CNS polarity. *Cell* **75,** 1417–1430 (1993).
7. Wilkinson, D. G., Bhatt, S. & Herrmann, B. G. Expression pattern of the mouse *T* gene and its role in mesoderm formation. *Nature* **343,** 657–659 (1990).
8. Irving, C., Nieto, A. A., DasGupta, R., Charnay, P. & Wilkinson, D. Progressive spatial restriction of *Sek-1* and *Krox-20* gene expression during hindbrain segmentation. *Dev. Biol.* **173,** 26–38 (1996).
9. Nieto, M. A., Gilardi-Hebenstreit, P., Charnay, P. & Wilkinson, D. G. A receptor protein tyrosine kinase implicated in the segmental patterning of the hindbrain and mesoderm. *Development* **116,** 1137–1150 (1992).
10. Takada, S. *et al. Wnt-3a* regulates somite and tailbud formation in the mouse embryo. *Genes Dev.* **8,** 174–189 (1994).
11. Bettenhausen, B., Hrabe de Angelis, M., Simon, S., Guenet, J.-L & Gossler, A. Transient and restricted expression during mouse embryogenesis of *Dll1*, a murine gene closely related to *Drosophila Delta*. *Development* **121,** 2407–2418 (1995).
12. Burgess, R., Cserjesi, P., Ligon, K. L. & Olson, E. N. Paraxis: a basic helix-loop-helix protein expressed in paraxial mesoderm and developing somites. *Dev. Biol.* **168,** 296–306 (1995).
13. Candia, A. F. *et al. Mox-1* and *Mox-2* define a novel homeobox gene subfamily and are differentially expressed during early mesodermal patterning in mouse embryos. *Development* **116,** 1123–1136 (1992).
14. Williams, B. A. & Ordahl, C. P. *Pax-3* expression in segmental mesoderm marks early stages in myogenic cell specification. *Development* **120,** 785–796 (1994).
15. Sasaski, H. & Hogan, B. L. M. Differential expression of multiple fork head-related genes during gastrulation and axial pattern formation in the mouse embryo. *Development* **118,** 47–59 (1993).
16. Walther, C. & Gruss, P. *Pax-6*, a murine paired box gene, is expressed in the developing CNS. *Development* **113,** 1435–1450 (1991).
17. Lewis, S. A. & Cowan, N. J. Genetics, evolution, and expression of the 68,000 mol. wt. neurofilament protein: isolation of a cloned cDNA probe. *J. Cell Biol.* **100,** 843–850 (1985).
18. Pfaff, S. L., Mendelsohn, M., Stewart, C. L., Edlund, T. & Jessell, T. M. Requirement for LIM homeobox gene *Isl1* in motor neuron generation reveals a motor neuron-dependent step in interneuron differentiation. *Cell* **84,** 309–320 (1996).
19. Tam, P. P. L. & Beddington, R. S. P. The formation of mesodermal tissues in the mouse embryo during gastrulation and early organogenesis. *Development* **99,** 109–126 (1987).
20. Yoshikawa, Y., Fujimori, T., McMahon, A. P. & Takada, S. Evidence that absence of *Wnt-3a* signaling promotes neuralization instead of paraxial mesoderm development in the mouse. *Dev. Biol.* **183,** 234–242 (1997).
21. Deng, C. *et al.* Fibroblast growth factor receptor-1 (FGFR-1) is essential for normal neural tube and limb development. *Dev. Biol.* **185,** 42–54 (1997).
22. Ciruna, B. G., Schwartz, L., Harpal, K., Yamaguchi, T. P. & Rossant, J. Chimeric analysis of *fibroblast growth factor receptor-1* (*Fgfr1*) function: a role for FGFR1 in morphogenetic movement through the primitive streak. *Development* **124,** 2829–2841 (1997).
23. Smith, J. *Brachyury* and the T-box genes. *Curr. Opin. Genet. Dev.* **7,** 474–480 (1997).
24. Nagy, A., Rossant, J., Nagy, R., Abramow-Newerly, W. & Roder, J. Derivation of completely cell culture-derived mice from early-passage embryonic stem cells. *Proc. Natl Acad. Sci. USA* **90,** 8424–8428 (1993).
25. Joyner, A. L. *Gene Targeting* (IRL, Oxford, New York, Tokyo, 1993).
26. Wilkinson, D. G. *Whole Mount In Situ Hybridization of Vertebrate Embryos* (IRL, Oxford, 1992).

Acknowledgements. We thank D. Wilkinson, T. Jessell, A. Gossler, E. Olson and B. Hogan for probes; P. Rodriguez, S. Campbell, C. Bogosian, B. Bogosian and P. Podikia for technical assistance; and T. Jessell, C. Stern, T. Bestor, L. Silver and members of our laboratory for contributions and suggestions. This work was supported by the Raymond and Beverly Sackler Foundation and by a grant from the NIH (to V.E.P.).

Correspondence and requests for materials should be addressed to V.E.P. (e-mail: vep1@columbia.edu).

Neural noise limitations on infant visual sensitivity

Ann M. Skoczenski & Anthony M. Norcia

Smith-Kettlewell Eye Research Institute, 2232 Webster Street, San Francisco, California 94115, USA

Visual contrast sensitivity is poor in newborn human infants, but improves rapidly to approach adult levels by 8 months of age[1–5]. During this period, infant sensitivity can be limited by physical factors affecting photon capture, such as eye size and photoreceptor density[6,7]. Here we show that infant visual sensitivity is also limited by high levels of noise in the neural transduction process. Using a non-invasive electrophysiological measurement[8–10] and a visual noise titration technique[11], we have found that intrinsic neural noise in neonates is approximately nine times higher than in adults. As intrinsic neural noise decreases during infancy, contrast sensitivity improves proportionally, suggesting that

neural noise places critical limits on contrast sensitivity throughout development. Moreover, contrast gain control[12], an inhibitory process that adjusts visual responses to changing stimulation, is in place and operating in infants as young as 6 weeks of age, in spite of high levels of neural noise and significant immaturities in contrast sensitivity. The contrast gain control that we observed in human neonates may serve as a building block for more complex forms of visual inhibition, which develop later in infancy[13].

Figure 1 illustrates the stimuli used in this study. Spatiotemporal noise reduces the visibility of patterns, making noise-embedded gratings (Fig. 1, right column) harder to resolve than gratings without added external noise (Fig. 1, left column). We calculated the effects of internal neural noise on contrast processing by titrating external stimulus noise and contrast thresholds. Thresholds were estimated in 32 infants and 5 adults by recording visually evoked potentials (VEPs) as a function of grating contrast for various levels of external spatiotemporal noise. Figure 2a shows examples of contrast response functions for a 1 cycle per degree sinewave grating, with and without added external noise, for three representative observers (two infants and one adult). The response to the grating stimulus increased monotonically with logarithmic contrast, and we estimated thresholds for grating visibility by extrapolating this curve to zero voltage[14]. This process was repeated for several levels of external noise, to produce a curve for each observer relating threshold to external noise. Threshold data and curves for the three representative observers are shown in Fig. 2b.

Each data set in Fig. 2b was fitted by a model that assumes summation of internal and external noise power[11]. According to this model, at low levels of external stimulus noise, the grating visibility threshold is determined by internal noise (the flat portion of each curve in Fig. 2b). When external noise exceeds the effects of internal noise, threshold is determined by external noise (rising portion of

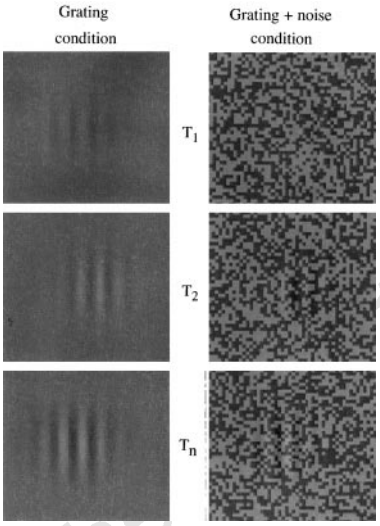

Figure 1 Schematic examples of the stimuli used in our experiments. Left column, three examples of a windowed sinewave grating with space-average luminance matched to the grey background. Grating contrast increases from top to bottom. Right column: the same three gratings with added two-dimensional noise. In our experiments, the grating stimulus was temporally modulated (contrast reversal) at a rate of 5.5 Hz to elicit visually evoked potentials. The stimulus noise was also temporally modulated, by refreshing interleaved noise frames at a rate of 33 Hz. During each 10-s 'sweep' trial, grating contrast increased logarithmically, while external noise contrast was fixed at a level between 0 and 0.40. The three left panels represent the stimulus at three points in time (T_1, T_2 and T_n) during a trial with no external noise added, and the three right panels represent the stimulus at three points in time during a trial with fixed-contrast added external noise.

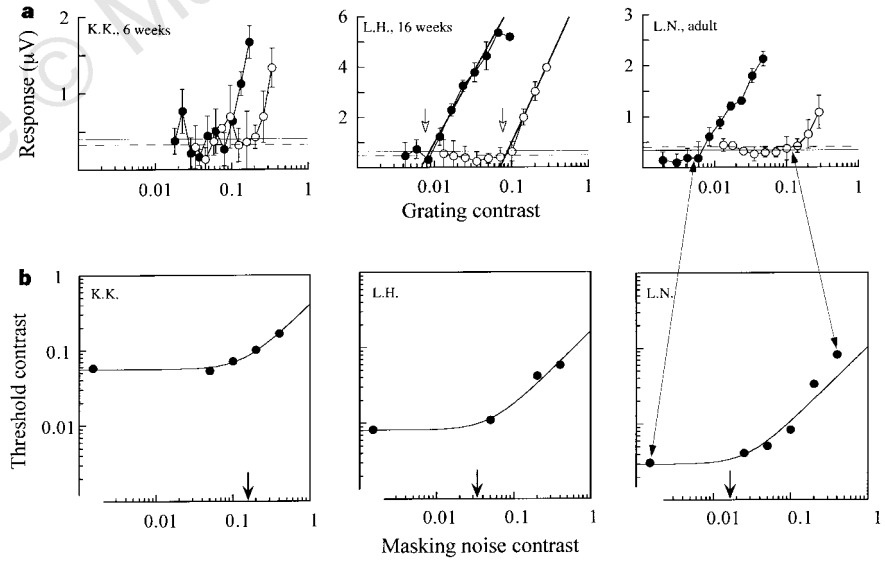

Figure 2 Data from three representative subjects: K.K., L.H. and L.N. **a**, 11.0 Hz visually evoked potential (VEP) response as a function of log grating contrast. Filled circles represent responses to the grating with no external stimulus noise added, and open circles represent responses to the grating plus external noise fixed at a contrast of 0.40. Solid and dotted horizontal lines in each plot indicate background EEG level (estimated from an average of responses at temporal frequencies just above and just below the VEP response frequency) for the no-noise and added-noise conditions, respectively. In all conditions, response increased monotonically with increasing grating contrast. Threshold was estimated by linear regression, extrapolating from the rising portion of the contrast response function to 0 μV, indicated by grey regression lines and arrows in the plot of observer L.H.'s data (see Methods for details). **b**, Contrast thresholds as a function of external noise contrast. Each datum represents a threshold estimate derived from a contrast response function based on 6–9 10-second sweep trials (two-headed arrows between the top and bottom plots of subject L.N.'s data identify two threshold estimates, **b**, and their related contrast response functions). The left-hand point in each plot represents the subject's threshold for a grating with no added noise. The function fitted to these data points is described by the equation $T = \sqrt{(N_s^2 + N_{eq}^2)}$, in which T is the contrast threshold for the grating with no external noise, N_s is external noise and N_{eq} is equivalent noise (representing the effects of internal neural noise)[11]. Each subject's N_{eq} is indicated by the arrow on the abscissa.

each curve). The intersection of these regions, called the equivalent noise (or N_{eq}, indicated by the arrow on each abscissa), indicates the level of external noise that raises the threshold by the same amount as the internal noise does. N_{eq} therefore represents the effects of internal visual noise on detection. This model provided a good fit to the data from each of our observers, and allowed us to estimate N_{eq} for individual observers.

For the youngest observer (aged 6 weeks) shown in Fig. 2b, both the contrast visibility threshold and the equivalent noise were higher than in the older infant (aged 16 weeks) and the adult. These data are representative of the developmental trends for threshold and equivalent noise in our group of observers. Figure 3a shows estimates of contrast threshold and N_{eq} as a function of age for 37 observers. The two measures follow a similar developmental timecourse, with N_{eq} consistently four to five times higher than contrast threshold throughout development.

Figure 3b shows threshold against N_{eq} for individual observers, and shows the strong relationship between the two measures. Threshold was significantly correlated with N_{eq} (correlation coefficient $(r) = 0.85$, $n = 41$, $P < 0.005$) across two log units of variation in contrast threshold. The best-fitting line relating the two measures had a slope of 1.04, and a non-parametric test showed that this was not significantly different from a slope of 1.0 ($P > 0.05$). This result is evidence that N_{eq} predicts contrast threshold, and moreover that the intrinsic neural noise represented by N_{eq} places critical limits on contrast thresholds in infants as well as adults.

What factors contribute to infants' elevated equivalent noise? The neural noise limiting our estimates of contrast threshold must arise somewhere before or within the cortical generator of the VEP. Elevated equivalent noise can, in principle, reflect reduced light capture (photon efficiency) by the infants' immature photoreceptors[6,15]. Poor photon efficiency is unlikely, however, to contribute significantly to our measures of equivalent noise as the infant VEP contrast threshold is unaffected by retinal illuminance over a 2-log-unit range for the luminance and spatiotemporal conditions used in the present experiments[16]. Adult contrast thresholds are also not limited by photon capture effects under the high luminance, low spatial frequency conditions used in our experiments[16,17]. Under these conditions, threshold is reached once a criterion signal-to-noise ratio is exceeded. Our estimate of equivalent noise reflects this internal noise level—rather than photon efficiency—as it changes during development.

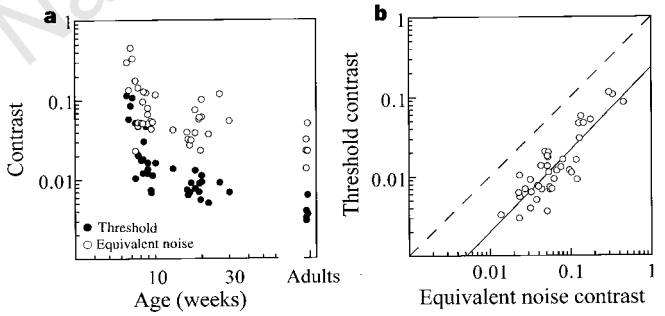

Figure 3 Relationship between contrast threshold, equivalent noise and age of subjects. **a**, Contrast threshold (filled circles) and equivalent noise contrast (open circles) as a function of age for 37 subjects. Contrast thresholds were estimated from an average of 6–9 trials. Equivalent noise was estimated from the equation in Fig. 2 fitted to 4–6 contrast thresholds measured at different levels of external noise. Both measures undergo an initial rapid phase of development between 6 and 10 weeks of age, followed by a more gradual phase of improvement. **b**, The relationship between contrast threshold and equivalent noise for individual subjects. The line of best fit to the data, with a slope of 1.1, is indicated by the solid line. The dashed line has a slope of 1.0; this slope would be expected if threshold is limited by equivalent noise.

We have also considered whether differences in background electroencephalogram (EEG) levels could have affected our measurements of equivalent noise. If EEG levels were higher in young infants, it might have been difficult to observe the visually driven signal at low contrasts. We find no significant difference, however, between background EEG levels in our youngest observers ($0.28 \pm 0.046\,\mu V$) and adults ($0.22 \pm 0.11\,\mu V$).

A consideration of VEP responses at suprathreshold contrasts constrains the location in the visual pathway where equivalent noise can be generated. Figure 2a shows contrast response functions with and without external noise for three observers of different ages. In all cases, high contrast external noise (at a level of 0.40) caused a rightward displacement of the contrast response function (on a log contrast axis), without altering the shape (slope) of the curve. This result implicates the functioning of a contrast scaling mechanism, a form of contrast gain control[12,18,19], which probably operates to maximize differential sensitivity (or visual discrimination) over the functional range of contrasts. Even the youngest infants in our sample had responses consistent with a functional contrast gain control mechanism. We see gain control effects as soon as the external noise exceeds the effects of internal neural noise, that is, for performance represented by the rising slopes of the curves in Fig. 2b. We can, therefore, infer that the neural noise limiting VEP contrast sensitivity is generated earlier in the visual pathway than the gain control mechanism.

Even with severe limits to absolute contrast sensitivity, the visual system of the neonate has an important qualitative similarity to the adult visual system: that is, the ability to adapt to changing conditions of stimulation. This early-developing contrast scaling is a form of visual inhibition: responses are reduced in the presence of high-contrast stimulation. Neural inhibition is thought to be an important factor in tuning visual responses to stimuli[20], and single-neuron studies of cats and monkeys have found evidence of inhibitory contrast gain control mechanisms at different stages of the visual pathway, from the retina to the cortex[12,18,19,21,22]. The contrast gain control that we observed in human infants may serve as a building block for more complex forms of inhibition, such as orientation-specific inhibition which does not develop until 6–8 months of age[13]. □

Methods

We recorded VEPs in 37 observers: 5 adults and 32 infants ranging in age from 6 to 30 weeks of age. Twenty-eight of the infants were tested in two sessions at one age, and the remaining four infants were each tested in four sessions at two ages. Subjects had no known visual abnormalities.

Test sinusoids and spatiotemporal noise were generated on alternating video frames using look-up table animation methods. The effective frame rate for both the grating and the noise patterns was 33.12 Hz. The test gratings were orientated vertically and were reversed in contrast at 5.5 Hz using a squarewave temporal modulation profile. Grating contrast was incremented over each 10-second trial in 10 equally spaced logarithmic steps that spanned the expected contrast threshold. The noise was created by random reassignment of lookup table values at the top of each noise frame. A total of 256 noise lookup tables was generated at the beginning of each trial. These tables were selected in a random sequence during each trial with no temporal periodicity. Spatially, the noise comprised a random element pattern whose individual elements were 9.2 arcmin on a side. Display contrast was linearized over an effective 12-bit range using an attenuation network[23]. Grating- and noise-frame crosstalk was measured with a fast photometer at <0.5%. Mean luminance was $100\,cd\,m^{-2}$ and the grating and noise patterns were co-extensive over a $15 \times 20°$ field.

Infant fixation was monitored by an experimenter who observed the centration of the corneal reflection of the test monitor. During each 10-s trial, the experimenter interrupted data collection if the infant lost fixation. Masked and unmasked stimulus trials were interleaved.

The EEG was digitized to 16-bits accuracy at 397 Hz over a 1–100 Hz passband (−6 dB). Three occipital derivations were used: C_z versus O_1, O_z and O_2 (international 10–20 system). The EEG obscures the observation of the

visual response as reflected in the VEP. Therefore, spectral analysis was performed using a recursive least-squares adaptive filter[24] to separate the VEP from the background EEG. The filter provided estimates of evoked response amplitude and phase over a 1 second running window. Six to nine individual 10-second trials were coherently averaged in the frequency domain to form averaged records of the Fourier amplitude of the second harmonic response (11 Hz) relative to the grating temporal frequency (5.5 Hz). Error statistics for averaged response amplitude were calculated using the T^2_{circ} statistic[25], which also provided statistical significance values for discriminating stimulus-driven VEPs from background EFG.

We estimated contrast thresholds from the averaged records by extrapolating the response versus contrast function to 0 μV using linear regression[14] (Fig. 2). The limits for the regression were selected using a combination of phase consistency and signal-to-noise ratio (SNR) criteria[8]. We calculated SNR on the basis of response amplitude and background EEG, the latter being estimated by averaging the EEG at two temporal frequencies, one just above and one just below the recording frequency. Background EEG amplitudes were not affected by visual stimulation: background levels remained constant throughout the 10-s sweep trials in both grating-alone and grating-plus-noise conditions, and the addition of external stimulus noise had no effect on background EEG levels (for example, for the youngest infants background EEG was 0.28 ± 0.046 microvolts in the grating-alone condition and 0.29 ± 0.042 microvolts in the condition with added high-contrast noise). Saturating portions of the contrast response function were excluded from the regression.

Received 15 August; accepted 4 November 1997.

1. Atkinson, J., Braddick, O. & Braddick, F. Acuity and contrast sensitivity of infant vision. *Nature* **247,** 403–404 (1974).
2. Harris, L., Atkinson, J. & Braddick, O. Visual contrast sensitivity of a 6-month-old infant measured by the evoked potential. *Nature* **264,** 570–571 (1976).
3. Norcia, A. M., Tyler, C. W. & Hamer, R. D. High visual contrast sensitivity in the young human infant. *Invest. Ophthalmol. Vis. Sci.* **29,** 44–49 (1988).
4. Norcia, A. M., Tyler, C. W. & Hamer, R. D. Development of contrast sensitivity in the human infant. *Vision Res.* **30,** 1475–1486 (1990).
5. Pirchio, M., Spinelli, D., Fiorentini, A. & Maffei, L. Infant contrast sensitivity evaluated by evoked potentials. *Brain Res.* **141,** 179–184 (1978).
6. Banks, M. S. & Bennett, P. J. Optical and photoreceptor immaturities limit spatial and chromatic vision of human neonates. *J. Opt. Soc. Am.* **5,** 2059–2079 (1988).
7. Wilson, H. R. Development of spatiotemporal mechanisms in the human infant. *Vision Res.* **28,** 611–628 (1988).
8. Norcia, A. M., Clarke, M. & Tyler, C. W. Digital filtering and robust regression techniques for estimating sensory thresholds from the evoked potential. *IEEE Engng Med. Biol.* **4,** 26–32 (1985).
9. Norcia, A. M., Tyler, C. W., Hamer, R. D. & Wesemann, W. Measurement of spatial contrast sensitivity with the swept contrast VEP. *Vision Res.* **29,** 627–637 (1989).
10. Tyler, C. W., Apkarian, P., Levi, D. M. & Nakayama, K. Rapid assessment of visual function: an electronic sweep technique for the pattern evoked potential. *Invest. Ophthalmol Vis. Sci.* **18,** 703–713 (1979).
11. Pelli, D. G. in *Vision: Coding and Efficiency* (ed. Blackmore, C.) 1–24 (Cambridge University Press, Cambridge, 1990).
12. Bonds, A. B. Temporal dynamics of contrast gain in single cells of the cat striate cortex. *Vis. Neurosci.* **6,** 239–255 (1991).
13. Morrone, M. C. & Burr, D. C. Evidence for the existence and development of visual inhibition in humans. *Nature* **321,** 235–237 (1986).
14. Campbell, F. W. & Maffei, L. Electrophysiological evidence for the existence of orientation and size detectors in the human visual system. *J. Physiol. (Lond.)* **207,** 635–652 (1970).
15. Yuodelis, C. & Hendrickson, A. A qualitative and quantitative analysis of the human fovea during development. *Vision Res.* **26,** 847–855 (1986).
16. Shannon, E., Skoczenski, A. M. & Banks, M. S. Retinal illuminance and contrast sensitivity in human infants. *Vision Res.* **36,** 67–76 (1996).
17. Van Nes, F. L. & Bouman, M. A. Spatial modulation transfer in the human eye. *J. Opt. Soc. Am.* **57,** 401–406 (1967).
18. Geisler, W. S. & Albrecht, D. G. Cortical neurons: isolation of contrast gain control. *Vision Res.* **32,** 1409–1410 (1992).
19. Ohzawa, I., Sclar, G. & Freeman, R. D. Contrast gain control in the cat's visual system. *J. Neurophysiol.* **54,** 651–667 (1985).
20. Burr, D. C. & Morrone, M. C. Inhibitory interactions in the human vision system revealed in pattern-evoked potentials. *J. Physiol. (Lond.)* **389,** 1–21 (1987).
21. Shapley, R. M. & Victor, J. D. The effect of contrast on the transfer properties of cat retinal ganglion cells. *J. Physiol. (Lond.)* **285,** 275–298 (1978).
22. Skoczenski, A. M., O'Keefe, L. P., Kiorpes, L., Tang, C., Hawken, M. J. & Movshon, J. A. Visual efficiency of macaque LGN neurons. *Neurosci. Abstr.* **20,** 7 (1994).
23. Pelli, D. G. & Zhang, L. Accurate control of contrast on microcomputer displays. *Vision Res.* **31,** 1337–1350 (1991).
24. Tang, Y. & Norcia, A. M. An adaptive filter for the steady-state VEP. *Electroencephalogr. Clin. Neurophysiol.* **96,** 268–277 (1994).
25. Victor, J. D. & Mast, J. A new statistic for steady-state evoked potentials. *Electroencephalogr. Clin. Neurophysiol.* **78,** 378–388 (1991).

Acknowledgements. This work was supported by the National Eye Institute and the Smith-Kettlewell Eye Research Institute. We thank D. C. Burr, N. V. Graham and J. A. Movshon for discussions, and the parents of our 32 infant subjects for volunteering their time.

Correspondence and requests for materials should be addressed to A.M.S. (e-mail: sko@skivs.ski.org).

Requirement for IRF-1 in the microenvironment supporting development of natural killer cells

Kouetsu Ogasawara*, Shigeaki Hida*, Nazli Azimi†, Yutaka Tagaya†, Takeo Sato*, Taeko Yokochi-Fukuda*, Thomas A. Waldmann†, Tadatsugu Taniguchi* & Shinsuke Taki*

** Department of Immunology, Graduate School of Medicine and Faculty of Medicine, University of Tokyo, Hongo 7-3-1, Bunkyo-ku, Tokyo 113, Japan*
† Metabolism Branch, National Cancer Institute, National Institutes of Health, Building 10, 9000 Rockville Pike, Bethesda, Maryland 20892, USA

Natural killer (NK) cells are critical for both innate and adaptive immunity[1,2]. The development of NK cells requires interactions between their progenitors and the bone-marrow microenvironment[3–6]; however, little is known about the molecular nature of such interactions. Mice that do not express the transcription factor interferon-regulatory factor-1 (IRF-1; such mice are IRF-1$^{-/-}$ mice) have been shown to exhibit a severe NK-cell deficiency[7,8]. Here we demonstrate that the lack of IRF-1 affects the radiation-resistant cells that constitute the microenvironment required for NK-cell development, but not the NK-cell progenitors themselves. We also show that IRF-1$^{-/-}$ bone-marrow cells can generate functional NK cells when cultured with the cytokine interleukin-15 (refs 9–12) and that the interleukin-15 gene is transcriptionally regulated by IRF-1. These results reveal, for the first time, a molecular mechanism by which the bone-marrow microenvironment supports NK-cell development.

In order to identify which cell population(s) is affected by IRF-1 deficiency, we first transferred bone-marrow cells from IRF-1$^{-/-}$ mice[13] that had been backcrossed several times with C57BL/6 (B6) mice into irradiated, H–2-compatible 129/SvJ (129) mice. In these chimaeric mice, donor-derived lymphoid cells can be distinguished from recipient lymphoid cells by the expression of Ly9.1, a marker protein that is expressed on lymphoid cells in 129 mice but not in B6 mice. As seen in Fig. 1a, irradiated 129 mice into which IRF-1$^{-/-}$ bone-marrow cells had been transferred (IRF-1$^{-/-}$ → 129 chimaeras) generated NK cells, which were defined by the expression of NK1.1 and lack of expression of Ly9.1 and CD3 on their surfaces. Similar numbers of NK cells were produced in IRF-1$^{-/-}$ → 129 chimaeras and control wild-type B6 → 129 chimaeras. Mononuclear cells isolated from mice reconstituted with either IRF-1$^{-/-}$ bone-marrow cells or control wild-type bone-marrow cells exhibited comparable cytotoxicity against NK-sensitive YAC-1 cells (Fig. 1b). Therefore, NK cells generated in IRF-1$^{-/-}$ → 129 chimaeras are functional. Complement-dependent elimination of NK cells using a monoclonal antibody against NK1.1 molecules (which is expressed by B6 but not by 129-derived NK cells) abolished cytotoxicity against YAC-1 cells, demonstrating that donor-derived NK cells are responsible for this cytotoxicity (data not shown). Hence, these results demonstrate that bone-marrow cells in IRF-1$^{-/-}$ mice are fully competent to differentiate into functional NK cells if an appropriate environment is provided by normal, radiation-resistant cells.

To confirm this, we transferred bone-marrow cells from 129 mice into irradiated IRF-1$^{-/-}$ mice. In this case NK cells were detected by their expression of Ly9.1 and the interleukin-2 receptor-β (IL-2Rβ) chain, another marker for NK cells[14]. As shown in Fig. 2a, 129 → IRF-1$^{-/-}$ chimaeras generated significantly fewer NK (Ly9.1$^+$IL-2Rβ$^+$CD3$^-$) cells than did control 129 → wild-type chi-